Magnetoelectric metglas/bidomain *y*+140°-cut lithium niobate composite for sensing fT magnetic fields

Andrei V. Turutin[1,2,a)], João V. Vidal[3], Ilya V. Kubasov[1], Alexander M. Kislyuk[1], Mikhail D. Malinkovich[1], Yurii N. Parkhomenko[1], Svetlana P. Kobeleva[1], Oleg V. Pakhomov[4], Andrei L. Kholkin[3,4], and Nikolai A. Sobolev[1,2]

[1] National University of Science and Technology MISIS, 119049 Moscow, Russia

[2] Department of Physics and I3N, University of Aveiro, 3810-193 Aveiro, Portugal

[3] Department of Physics and CICECO - Aveiro Institute of Materials, University of Aveiro, 3810-193 Aveiro, Portugal

[4] ITMO University, Laboratory "Materials and Structures for Electro- and Magnetocaloric Energy Conversion", 197101 St. Petersburg, Russia

We investigated the magnetoelectric properties of a new laminate composite material based on *y*+140°-cut congruent lithium niobate piezoelectric plates with an antiparallel polarized "head-to-head" bidomain structure and metglas used as a magnetostrictive layer. A series of bidomain lithium niobate crystals were prepared by annealing under conditions of Li_2O outdiffusion from $LiNbO_3$ with a resultant growth of an inversion domain. The measured quasi-static magnetoelectric coupling coefficient achieved $|\alpha_{E31}| = 1.9$ V·(cm·Oe)$^{-1}$. At a bending resonance frequency of 6862 Hz, we found a giant $|\alpha_{E31}|$ value up to 1704 V·(cm·Oe)$^{-1}$. Furthermore, the equivalent magnetic noise spectral density of the investigated composite material was only 92 fT/Hz$^{1/2}$, a record value for such a low operation frequency. The magnetic-field detection limit of the laminated composite was found to be as low as 200 fT in direct measurements without any additional shielding from external noises.

Composite magnetoelectric (ME) materials have gained great interest in recent years because of their possible applications in ultra-sensitive magnetic sensors, energy harvesters, low power consumption memory devices, microwave phase shifters, gyrators, etc. [1−6]. In our research we are focused on low-frequency, ultra-sensitive magnetic field sensors with the aim of using them in biomedicine, e.g., in magnetoencephalography and magnetocardiography [2,7,8]. The absence of the need to cool such sensors is a significant technical advantage over the currently used superconducting quantum interferometers (SQUIDs). Obviously, magnetic field sensors based on composite multiferroics cannot fully replace SQUIDs capable of detecting single magnetic flux quanta. At the moment, the best equivalent magnetic noise spectral density (EMND) value for ME sensors based on simple ME 2-2 laminate composites containing mechanically coupled magnetostrictive (MS) and piezoelectric (PE) layers [9] reported in the literature are of the order of 1 pT/Hz$^{1/2}$ for an operation frequency of 10 Hz [10–12]. In comparison, SQUID, fluxgate and magneto-impedance sensors have equivalent noise levels of the order of 1 fT/Hz$^{1/2}$ [13], 5 pT/Hz$^{1/2}$ [14], and 10 pT/Hz$^{1/2}$ [15] at 10 Hz, respectively.

The majority of scientific groups engaged in the manufacture of composite multiferroics and studies of their properties are using materials based on PE ceramics such as PZT or PMN–PT ferroelectric relaxors. Despite their outstanding PE characteristics, these materials have a number of drawbacks, such as a low Curie temperature, considerable mechanoelectric hysteresis, creep (time delay and saturation between mechanical deformation and electric signal), nonlinear behavior, strong dependence of the properties on the temperature, as well as large dielectric losses. One possible approach to improve these parameters is to use lead-free PE single crystals such as lithium

a) Correspondence should be addressed to a.turutin@misis.ru

niobate with high voltage piezoelectric coefficients (g), low permittivity and very low mechanical and dielectric losses [16–21]. Furthermore, asymmetric bi-layered systems with bimorph PEs, containing two oppositely poled layers along the thickness direction, are able to generate large voltages under a low-frequency bending deformation and partially cancel both extrinsic vibrational and thermal noises [8,22].

Recently we have shown the possibility to produce large ME effects in composites containing lead-free congruent LiNbO$_3$ (LNC) single crystals [16,17,20]. Furthermore, some new promising techniques have been developed to directly engineer two ferroelectric domains with antiparallel spontaneous polarization vectors in a single crystal plate (bidomain) [23,24]. In a previous studies we proposed the use of square or long bar metglas / PE bi-layered composites with y+128°-cut LNC single-crystal "head-to-head" (H–H) and "tail-to-tail" (T–T) bidomains in sensitive magnetic field sensors [18,19].

The anisotropy of single-crystalline LNC can be used to achieve a high direction-dependent sensitivity to magnetic fields at low frequencies. Choosing a crystal with an appropriate cut is a very important step in the development of the ME sensors. Figure 1 shows the representation surface of the maximum absolute in-plane piezoelectric coefficient $|d_{3j}|$ as a function of the crystal cut orientation calculated using the material constants found in the literature [25]. We observe a very large variation of the transversal PE coefficients with the orientation of the PE crystal, whose symmetry coincides with the symmetry of the corresponding crystal's point group [26]. There are six directions with a transversal d_{31} constant of 15.38 pm/V for a crystal with the y+140°-cut and two equivalent cuts conditioned by 3m symmetry. The in-plane piezoelectric g_{31} coefficient equals $\varepsilon_{31}^{-1}d_{31}$, which is proportional to the bending open-circuit voltage ME coefficient in the bidomain composite, follows an equivalent trend being as large as 19.11 m·mV/N for this same cut, thus being comparable to the maximum values found, e.g., in PZT and PMN–PT [27]. Moreover, the y+140°-cut is very close to the y+137°-cut that yields a maximum transverse electromechanical coupling factor of 0.51 [28]. Other crystal cuts possibly interesting for direction-sensitive applications are e.g. the y-cut corresponding to the unipolar regime ($d_{31} = -20.8$ pm/V and $d_{32} = 0$), the y+26.5°-cut corresponding to the in-plane isotropic regime ($d_{31} = d_{32} = -18.9$ pm/V), and the y+162°-cut corresponding to the anisotropic bipolar regime ($d_{31} = -d_{32} = 19.6$ pm/V).
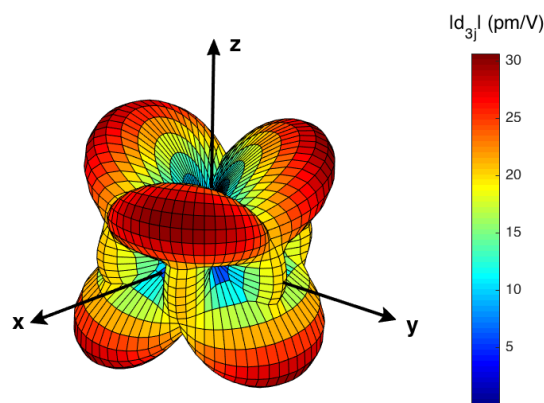

FIG. 1. (color online) Representation surface of the maximum absolute in-plane PE coefficient $|d_{3j}|$ as a function of the crystal orientation of the LNC single crystal (x, y, z are the crystal axes chosen in the same manner as in Refs. [29–31]).

As the PE phase in the ME composites we used single-domain LNC crystal plates with a y+140°-cut sliced from a boule with a congruent composition (JSC "Fomos-Materials", Russia).

The surfaces of the plates were grinded using a diamond disc in order to obtain a thickness of 410 μm; the surface roughness was of the order of 5 μm. Finally, we cut several long-bar samples from the plates with a length of 20 mm and a width of 5 mm.

We used the so-called diffusion annealing (DA) technique [32–34] in order to form a ferroelectric "head-to-head" bidomain structure in the LNC plates. For this purpose, we annealed the crystals in an air ambient at a temperature of 1100ºC for 5 hours in order to achieve an out-diffusion of Li_2O accompanied by a polarization inversion. All the samples were heat treated during one and the same annealing process. An angle lap of one of the samples was prepared and etched in a HF : HNO_3 = 2 : 1 (vol.) mixture for the visualization of the domain structure according to Ref. [35]. As it is clearly seen in Figure 2(a), 5 hours are sufficient for a polarization reversal in a half of the sample. A certain inclination of the domain interface near the left and right edges of the angle lap is a result of the diffusion anisotropy in LNC.
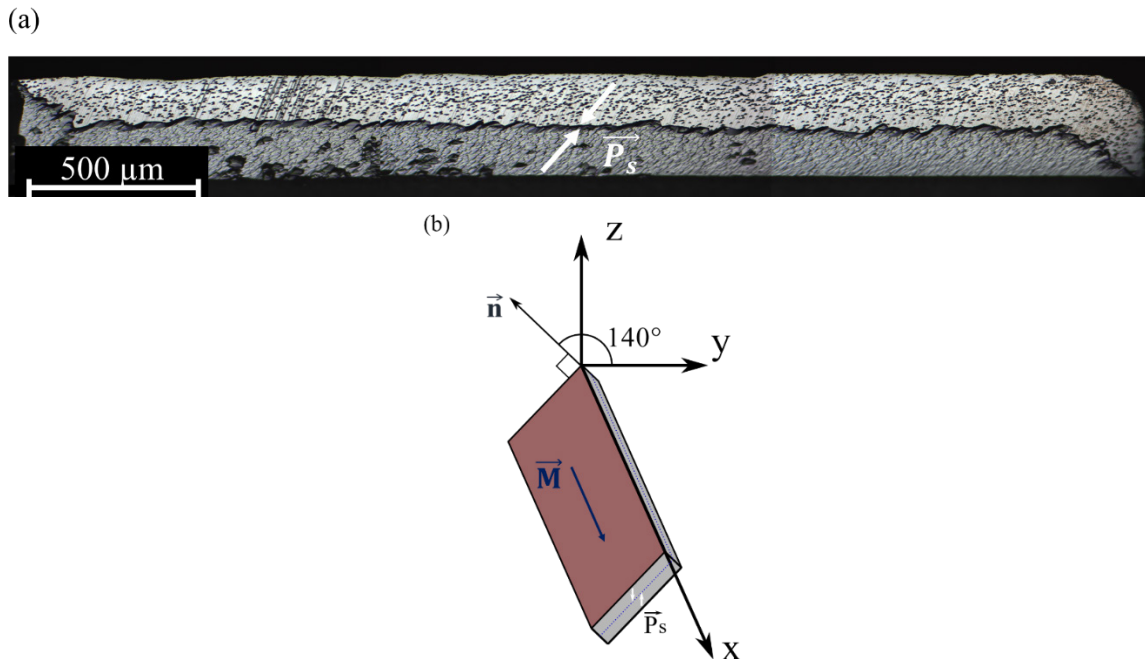
(a)

(b)

FIG. 2. (color online) (a) Photograph of an etched angle lap of a $y+140°$-cut bidomain LNC crystal. (b) Scheme of the ME bi-layered long-bar composite formed by a top MS layer and a bottom PE bidomain single crystal, where the white arrows represent the vectors of spontaneous polarization ($\overrightarrow{P_S}$) in the "head-to-head" (H–H) domain structure. The black arrows indicate the x, y, z crystal axes and the cut angle.

The method of domain structure control by etched angle lap is destructive for the sample. To avoid this, we next used another technique in order to select the best bidomain sample. It is known that bidomain LNC crystals bend according to the bimorph principle [36–38], when an external electric field is applied. The equation describing the deflection of the end of the cantilevered bimorph predicts its linear dependence on the piezoelectric coefficient and the applied voltage, as well as a quadratic dependence on the L/t factor [39]: $\delta = k \cdot U \left(\frac{L}{t}\right)^2$, where L and t are the length and thickness of the bimorph, respectively, U is the applied voltage, and $k = 1.5 \cdot d_{31}$ in the case of an ideal bimorph. For the $y+140°$-cut we should have $k_{y+140°} = 23.17$ pm/V. However, due to the non-ideality of the domain interface in the center of the bidomain crystal [23,24], the real k will be smaller, thus reducing the deflection of the cantilevered bimorph end (δ). As we can measure L and

t directly, and $\delta = f(U)$ is a linear function with a fixed slope, it is easy to calculate *k* and compare it to the theoretical prediction.

After the bidomain structure formation, nickel electrodes with a thickness of ca. 100 nm were deposited on the polar surfaces of the crystals by magnetron sputtering in order to create a bimorph actuator. For the purpose of the measurement of δ as a function of the applied voltage *U*, a homemade clamping tool was used. The deflection of the free cantilever end was controlled by an optical microscope ZEISS Axio Imager M1 as described in Ref. [26] The voltage across the bimorph was changing step by step from -500 V to $+500$ V, and measurements of δ were performed every 50 V. The resulting points were fitted by a straight line with a slope = δ/U. Finally, we calculated the *k* coefficients of the bimorphs.

The best of our samples had $k = 20.2$ pm/V which is only 13% lower than the theoretically predicted value. Other samples had a lower quality ($k < 18$ pm/V), possibly due to domain structure artifacts or a decrease of the PE coefficients as a result of the lithium oxide depletion of the crystals [40]. Only the best bidomain crystal was used in the magnetoelectric and impedance measurements.

Here we report a 2–2 connectivity L–T ME thin composite consisting of a bidomain LNC *y*+140°-cut single crystal and a commercial 2826MB type ($Fe_{0.4–0.5}Ni_{0.4–0.5}Mo_{0.05–0.1}B_{0.01–0.05}$) metglas foil (Hitachi Metals Europe GmbH) which were bonded together using an aerospace epoxy adhesive (3M™ Scotch–Weld™ Epoxy Adhesive EC–2216 B/A). The composite was subsequently cured at 66ºC for 2 hours under a vertical pressure of 100 kPa uniformly applied over the entire area of the sample by a piston cylinder. The dimensions of the sample were as follows: length = 20 mm, width = 5 mm, thickness of the PE phase = 410 μm, thickness of the MS phase = 29 μm. The scheme of the composite ME sample is shown in Figure 2(b).

Measurements of the impedance, voltage noise density and dynamic direct ME effect were performed in the range from $f = 1$ Hz to $f = 10$ kHz at room temperature in the free vibrating regime, where the sample placed in the measurement setup was supported in its center by thin flexible nonmagnetic wires. The measurements were carried out using a high input impedance and low input noise lock-in differential amplifier (Zurich Instruments®, MFLI). A homemade setup was used in the ME measurements consisting of six collinear Helmholtz coils, four of which produce a small amplitude modulation AC field (δH) and two outer ones create a highly homogeneous DC bias magnetic field (H) across the whole volume of the sample. The quasi-static ME measurements were executed at a frequency of $f = 110$ Hz, far from resonance, while applying a modulation AC magnetic field of $\delta H = 0.1$ Oe in a range of bias fields H_{bias} from -25 Oe to $+25$ Oe. The resonant ME measurements were performed as a function of the frequency with a constant field of $\delta H = 0.01$ Oe and a bias corresponding to the maximum of the quasi-static effect. The ME coefficient was calculated as $\alpha_{E31} = \delta V_{ME}/(t_p \cdot \delta H)$.

For the characterisation of its noise density, the sample was placed inside a grounded aluminum box shielded from environmental vibrations and other extrinsic electromagnetic noise sources. The noise from the composite was measured by the lock-in operating in its lowest 1 mV input range, with a bandwidth of the input filter of 1 Hz and without any applied AC magnetic field, using the noise-measuring mode of the device. The obtained results were expressed in terms of the voltage noise spectral density in units of $V/Hz^{1/2}$, which corresponds to the root mean square value of the measured voltage amplitude normalized by the square root of the bandwidth of the input filter. The equivalent magnetic noise spectral density and limit of detection of the ME sensor were measured using a bandwidth of the input filter of $\Delta f = 1$ Hz. The practical sensitivity of the sample

was measured as a function of the AC magnetic field in resonance conditions with applying DC bias magnetic field which corresponds to the maximum of the ME effect in quasi-static conditions. The measurements were performed without any additional shielding from external noise sources.

The measured impedance spectra of the thin-bar ME metglas / bidomain y+140º-cut LNC composite and of the PE bidomain $y+140^o$-cut LNC crystal alone operating in a free vibrating regime are shown in Figure 3(a). Superimposed are the calculated results obtained using a simple unidimensional ME model [18,19]. The resonance and antiresonance peaks are associated with low-frequency bending electromechanical modes (EMR). The main electromechanical parameters of the PE crystal / ME composite such as the low-frequency capacitance C, dielectric loss tangent $\tan(\delta)$ (measured at 1 kHz), resonance frequencies f_r and f_a and mechanical quality factor Q of the fundamental resonance mode have been obtained from these spectra. They are summarized in Table I. The dielectric loss tangents are shown to be quite low, $tan(\delta) \sim 1.3\%$. The mechanical quality factors, calculated as the ratio between the resonance frequency and the full width at half maximum of the real admittance Y' peaks, take large values of $Q \sim 1100$ in the ME composite, whereas in the PE crystal alone we have $Q \sim 1200$. This difference can be explained by taking into account additional damping losses introduced by the intermediate layer of viscous epoxy and the MS phase. The Nyquist plots of the active (Z') and reactive (Z'') parts of the impedance near the antiresonance frequency of the fundamental bending mode measured in the ME composite and PE crystal are presented in Figure 3(b). In the calculations a simple analytical unidimensional dynamic model based on the linear theory of piezoelectricity and magnetostriction applied to ME composite thin bar was employed assuming typical values of $tan(\delta) = 1\%$ and $Q = 1100$.
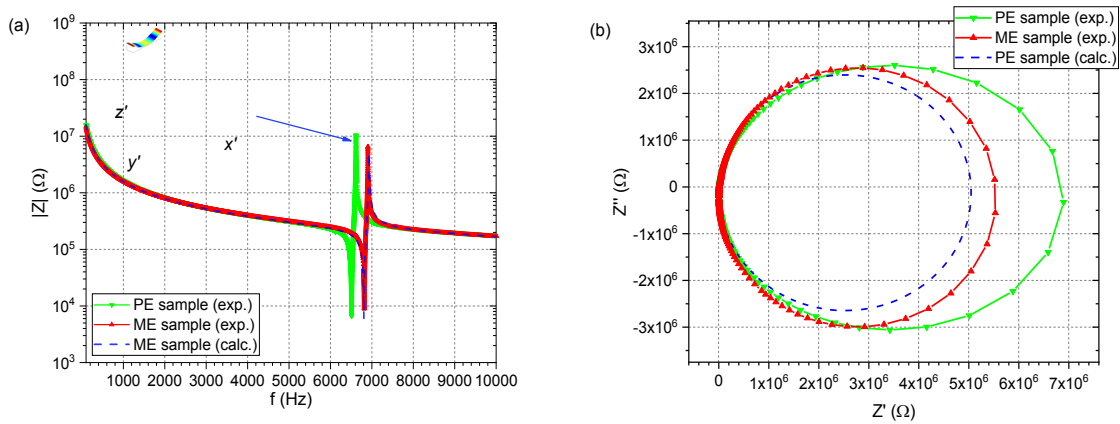

FIG. 3. (color online) (a) Impedance spectra of the measured bidomain $y+140$-cut LNC crystal, ME composite of metglas / $y+140$-cut LNC, as well as theoretically calculated spectra. The inset shows the spatial deformation of the PE crystal under its fundamental bending mode which corresponds to the antiresonance frequency, where the impedance and averaged strain (i.e. overall deformation) under open-circuit conditions are maximized. (b) Nyquist plots of the active (Z') and reactive (Z'') parts of the impedance for the PE crystal and ME composite, together with the calculated curve.

Measurements of the direct ME effect were carried out at room temperature and at a frequency of 110 Hz in the quasi-static regime with an applied modulation magnetic field of $\delta H = 0.1$ Oe. Figure 4(a) shows the result of the quasi-static measurement of the transversal ME coefficient as a function of the applied in-plane bias field. Using a low-frequency model [18,19], the maximum expected quasi-static ME coefficient of $|\alpha_{E31}| = 5.4$ V·(cm·Oe)$^{-1}$ was calculated. The maximum measured quasi-static ME coefficient was as large as $|\alpha_{E31}| = 1.9$ V·(cm·Oe)$^{-1}$. The big

difference between the calculated and experimental values can be explained by an imperfect mechanical coupling between the MS and PE phases due to the viscous intermediate epoxy layer and interdomain region in the bidomain crystal, which negatively influences the quality of the latter. The ME sample is also shown to exhibit a nonhysteretic behaviour which is characteristic of the used PE and MS phases.
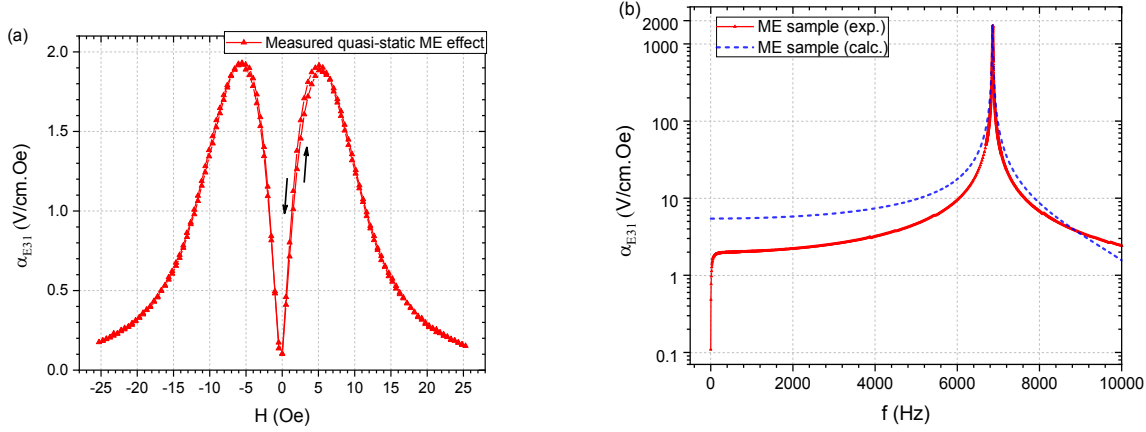

FIG. 4. (color online) (a) Quasi-static in-plane direct ME coefficient ($|\alpha_{E31}|$) measured as a function of the magnetic bias field H at $f = 110$ Hz and with an AC modulation magnetic field of $\delta H = 0.1$ Oe. (b) Dynamic ME effect frequency response of the investigated sample measured with the optimal DC bias field H = 5 Oe and modulation field $\delta H = 0.01$ Oe, as well as a calculated curve.

The dynamic ME coefficient was measured as a function of the modulation frequency with an applied optimum bias field of 5 Oe corresponding to the maximum ME effect, as measured in the quasi-static regime. As we see in figure 4(b), a giant bending resonance ME coefficient of up to 1704 V·(cm·Oe)$^{-1}$ was obtained at 6862 Hz. This strong peak corresponds to the antiresonance frequency of the bending mode.
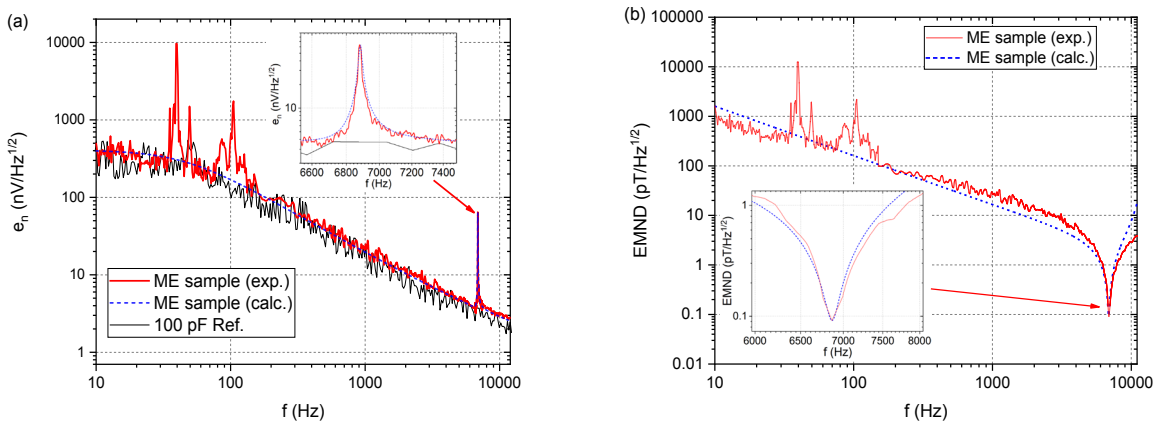

FIG. 5. (color online) (a) Voltage noise spectral density (e_n) measured in the ME metglas / bidomain y+140°-cut LNC composite as a function of the frequency. Demonstrated are also the results of the measured input voltage noise of the lock-in amplifier connected to a reference 100 pF capacitor, as well as the noise spectra calculated using a unidimensional model. (b) Equivalent magnetic noise spectral density (EMND) measured as a function of the frequency in the metglas / y+140°-cut LNC composite, as well as a calculated curve.

To show the best low-frequency magnetic-field detectivity of the ME metglas / bidomain *y*+140°-cut LNC composite, measurements of the equivalent voltage noise density (e_n) of the sample and detection circuit were performed (Figure 5(a)). These were made using the same setup as in the ME measurements, while shielding the system from external magnetic, acoustic and vibrating noises. Furthermore, a reference 100 pF capacitor was measured in order to show the voltage noise density floor of the detection circuit. The calculated curve was obtained taking into account the impedance thermal Jonhson-Nyquist noise $(4 \cdot k_b \cdot T \cdot Z')^{1/2}$ of the sensor while operating at room temperature [18,19]. The calculated e_n values are shown to be as low as 63 nV/Hz$^{1/2}$ at the resonance frequency of 6862 Hz. The measured resonance peak of the voltage noise density in the sample equaled 64 nV/Hz$^{1/2}$. In order to quantify the detection capabilities of the sensor we calculated its resultant equivalent magnetic noise spectral density EMND $= e_n/(\alpha_{E31} \cdot t_p)$, as shown in Figure 5(b). The ME composite thus exhibits a giant conversion factor of 69.9 V/Oe at resonance, and the correspondent magnetic noise density is quite low – only 92 fT/Hz$^{1/2}$ at a frequency of 6862 Hz.
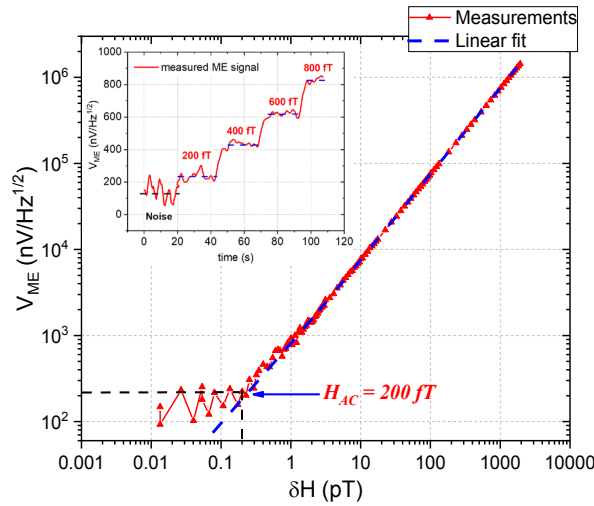

FIG. 6. (color online) Magnetic-field detection limit and linear output voltage response of the sensor to an AC magnetic field *δH* varying from 0.015 pT to 2000 pT at the resonance frequency of 6862 Hz with the applied H$_{bias}$ = 5 Oe.

Table I. Summary of the experimental and calculated electromechanical parameters of the ME and PE samples. Here, C and $\tan(\delta)$ are the low-frequency (1 kHz) parallel capacitance and loss tangent, f_r and f_a are the resonance and antiresonance frequencies of the fundamental electromechanical bending mode, Q is the mechanical quality factor, $|\alpha_{E31}|$ are the ME coefficients measured under quasi-static (at 110 Hz) and resonant (at f_a) conditions, as well as the EMND.

	ME sample (exp.)	ME sample (calc.)	PE sample (exp.)
C, pF	99	100	88
$\tan(\delta)$, %	1.3	1	0.6
f_r, Hz	6810	6806	6512
f_a, Hz	6862	6862	6617
Q	1105	1100	1208
$|\alpha_{E31}(110 \text{ Hz})|$, V·(cm·Oe)$^{-1}$	1.9	5.4	–
$|\alpha_{E31}(f_a)|$, V·(cm·Oe)$^{-1}$	1704	1707	–
EMND(f_a), fT/Hz$^{1/2}$	92	90	–

Finally, we tested the magnetic-field sensitivity of the ME composite at its resonant frequency by measuring the output voltage from the detection circuit as a function of the amplitude of an applied AC magnetic field. These results are presented in Figure 6 and were obtained under real-life conditions. It can be seen that the ME sample exhibits a considerable sensitivity to very weak AC magnetic fields. The smallest detectable ME signal corresponds to $\delta H = 200$ fT at a resonance frequency of 6862 Hz. Subsequently, the voltage is shown to increase very linearly with the field amplitude at a ratio of 69.9 V/Oe.

In summary, experimental results of the ME effect and AC magnetic-field sensitivity measurements in a laminate composite comprising a bidomain $y+140°$-cut LNC single crystal and metglas are reported. The experimentally obtained ME coefficient was as large as 1704 V·(cm·Oe)$^{-1}$. A very small AC magnetic field of 200 fT could be detected under resonance conditions in direct measurements without any additional shielding from external noises. Furthermore, the EMND of the investigated composite is only of 92 fT/Hz$^{1/2}$, which is a record value for an operation frequency as low as 6.86 kHz [41–43]. This result is quite competitive with the best recently developed ME sensors with a minimum magnetic noise of ca. 135 fT/Hz$^{1/2}$ at a higher resonance frequency of 23.23 kHz [41]. Besides, we have observed a good correspondence between the experimental results and those calculated with the help of a unidimensional model. Thus, such a ME composite material might find use in lead-free sensitive room-temperature low-frequency magnetic sensors, e.g. for biomedical applications.

References

1. Vopson, M. M. Fundamentals of Multiferroic Materials and Their Possible Applications. *Crit. Rev. Solid State Mater. Sci.* **2015**, *40*, 223–250, doi:10.1080/10408436.2014.992584.
2. Röbisch, V.; Salzer, S.; Urs, N. O.; Reermann, J.; Yarar, E.; Piorra, A.; Kirchhof, C.; Lage, E.; Höft, M.; Schmidt, G. U.; Knöchel, R.; McCord, J.; Quandt, E.; Meyners, D. Pushing the detection limit of thin film magnetoelectric heterostructures. *J. Mater. Res.* **2017**, *32*, 1009–1019, doi:10.1557/jmr.2017.58.
3. Wang, Y.; Li, J.; Viehland, D. Magnetoelectrics for magnetic sensor applications: status, challenges and perspectives.

Mater. Today **2014**, *17*, 269–275, doi:https://doi.org/10.1016/j.mattod.2014.05.004.

4. Palneedi, H.; Annapureddy, V.; Priya, S.; Ryu, J. Status and Perspectives of Multiferroic Magnetoelectric Composite Materials and Applications. *Actuators* **2016**, *5*, 9, doi:10.3390/act5010009.

5. Sun, N. X.; Srinivasan, G. Voltage Control of Magnetism in Multiferroic Heterostructures and Devices. *Spin* **2012**, *02*, 1240004, doi:10.1142/S2010324712400048.

6. Zhai, J.; Li, J.; Dong, S.; Viehland, D.; Bichurin, M. I. A quasi(unidirectional) Tellegen gyrator. *J. Appl. Phys.* **2006**, *100*, 124509, doi:10.1063/1.2402967.

7. Salzer, S.; Röbisch, V.; Klug, M.; Durdaut, P.; McCord, J.; Meyners, D.; Reermann, J.; Höft, M.; Knöchel, R. Noise Limits in Thin-Film Magnetoelectric Sensors With Magnetic Frequency Conversion. *IEEE Sens. J.* **2018**, *18*, 596–604, doi:10.1109/JSEN.2017.2776039.

8. Zhai, J.; Xing, Z.; Dong, S.; Li, J.; Viehland, D. Detection of pico-Tesla magnetic fields using magneto-electric sensors at room temperature. *Appl. Phys. Lett.* **2006**, *88*, 62510, doi:10.1063/1.2172706.

9. Nan, C.-W.; Bichurin, M. I.; Dong, S.; Viehland, D.; Srinivasan, G. Multiferroic magnetoelectric composites: Historical perspective, status, and future directions. *J. Appl. Phys.* **2008**, *103*, 31101, doi:https://doi.org/10.1063/1.2836410.

10. Wang, Y.; Li, M.; Hasanyan, D.; Gao, J.; Li, J.; Viehland, D. Geometry-induced magnetoelectric effect enhancement and noise floor reduction in Metglas/piezofiber sensors. *Appl. Phys. Lett.* **2012**, *101*, 92905, doi:10.1063/1.4737906.

11. Yaojin, W.; David, G.; David, B.; Junqi, G.; Menghui, L.; Jiefang, L.; Dwight, V. An Extremely Low Equivalent Magnetic Noise Magnetoelectric Sensor. *Adv. Mater.* **2011**, *23*, 4111–4114, doi:10.1002/adma.201100773.

12. Gao, J.; Das, J.; Xing, Z.; Li, J.; Viehland, D. Comparison of noise floor and sensitivity for different magnetoelectric laminates. *J. Appl. Phys.* **2010**, *108*, 84509, doi:10.1063/1.3486483.

13. Sternickel, K.; Braginski, A. I. Biomagnetism using SQUIDs: Status and perspectives. *Supercond. Sci. Technol.* **2006**, *19*, S160, doi:10.1088/0953-2048/19/3/024.

14. Karo, H.; Sasada, I. Magnetocardiogram measured by fundamental mode orthogonal fluxgate array. *J. Appl. Phys.* **2015**, *117*, 17B322, doi:10.1063/1.4918958.

15. Nakayama, S.; Uchiyama, T. Real-time Measurement of Biomagnetic Vector Fields in Functional Syncytium Using Amorphous Metal. *Sci. Rep.* **2015**, *5*, 8837.

16. Timopheev, A. A.; Vidal, J. V; Kholkin, A. L.; Sobolev, N. A. Direct and converse magnetoelectric effects in Metglas/LiNbO3/Metglas trilayers. *J. Appl. Phys.* **2013**, *114*, 44102, doi:10.1063/1.4816400.

17. Vidal, J. V; Timopheev, A. A.; Kholkin, A. L.; Sobolev, N. A. Anisotropy of the magnetoelectric effect in tri-layered composites based on single-crystalline piezoelectrics. *Vacuum* **2015**, *122*, 286–292, doi:https://doi.org/10.1016/j.vacuum.2015.06.022.

18. Vidal, J. V.; Turutin, A. V.; Kubasov, I. V.; Malinkovich, M. D.; Parkhomenko, Y. N.; Kobeleva, S. P.; Kholkin, A. L.; Sobolev, N. A. Equivalent Magnetic Noise in Magnetoelectric Laminates Comprising Bidomain LiNbO3 Crystals. *IEEE Trans. Ultrason. Ferroelectr. Freq. Control* **2017**, *64*, 1102–1119, doi:10.1109/TUFFC.2017.2694342.

19. Turutin, A. V.; Vidal, J. V; Kubasov, I. V; Kislyuk, A. M.; Malinkovich, M. D.; Parkhomenko, Y. N.; Kobeleva, S. P.; Kholkin, A. L.; Sobolev, N. A. Low-frequency magnetic sensing by magnetoelectric metglas/bidomain LiNbO3 long bars. *J. Phys. D: Appl. Phys.* **2018**, *51*, 214001, doi:10.1088/1361-6463/aabda4.

20. Vidal, J. V; Timopheev, A. A.; Kholkin, A. L.; Sobolev, N. A. Dynamic Measurements of Magnetoelectricity in Metglas-Piezocrystal Laminates BT - Nanostructures and Thin Films for Multifunctional Applications: Technology, Properties and Devices. In *Nanostructures and Thin Films for Multifunctional Applications*; Tiginyanu, I., Topala, P., Ursaki, V., Eds.; Springer International Publishing: Cham, 2016; pp. 227–265 ISBN 978-3-319-30198-3.

21. Vidal, J. V; Timopheev, A. A.; Kholkin, A. L.; Sobolev, N. A. Engineering the Magnetoelectric Response in Piezocrystal-Based Magnetoelectrics: Basic Theory, Choice of Materials, Model Calculations BT - Nanostructures and Thin Films for Multifunctional Applications: Technology, Properties and Devices. In *Nanostructures and Thin Films for Multifunctional Applications*; Tiginyanu, I., Topala, P., Ursaki, V., Eds.; Springer International Publishing: Cham, 2016; pp. 189–226 ISBN 978-3-319-30198-3.

22. Xing, Z.; Zhai, J.; Li, J.; Viehland, D. Investigation of external noise and its rejection in magnetoelectric sensor design. *J. Appl. Phys.* **2009**, *106*, 24512, doi:10.1063/1.3176500.

23. Kubasov, I. V; Timshina, M. S.; Kiselev, D. A.; Malinkovich, M. D.; Bykov, A. S.; Parkhomenko, Y. N. Interdomain region in single-crystal lithium niobate bimorph actuators produced by light annealing. *Crystallogr. Reports* **2015**, *60*, 700–705, doi:10.1134/S1063774515040136.

24. Kubasov, I. V; Kislyuk, A. M.; Bykov, A. S.; Malinkovich, M. D.; Zhukov, R. N.; Kiselev, D. A.; Ksenich, S. V; Temirov, A. A.; Timushkin, N. G.; Parkhomenko, Y. N. Bidomain structures formed in lithium niobate and lithium tantalate single crystals by light annealing. *Crystallogr. Reports* **2016**, *61*, 258–262, doi:10.1134/S1063774516020115.

25. Warner, A. W.; Onoe, M.; Coquin, G. A. Determination of Elastic and Piezoelectric Constants for Crystals in Class (3m). *J. Acoust. Soc. Am.* **1967**, *42*, 1223–1231, doi:10.1121/1.1910709.

26. Kubasov, I. V; Popov, A. V; Bykova, A. S.; Temirov, A. A.; Kislyuk, A. M.; Zhukov, R. N.; Kiselev, D. A.; Chichkov, M. V; Malinkovich, M. D.; Parkhomenko, Y. N. Deformation Anisotropy of Y + 128°-Cut Single Crystalline Bidomain Wafers of Lithium Niobate. *Russ. Microelectron.* **2017**, *46*, 557–563, doi:10.1134/S1063739717080108.

27. Sreenivasulu, G.; Petrov, V. M.; Fetisov, L. Y.; Fetisov, Y. K.; Srinivasan, G. Magnetoelectric interactions in layered composites of piezoelectric quartz and magnetostrictive alloys. *Phys. Rev. B* **2012**, *86*, 214405.

28. Shimizu, K. N. and H. A. and H. Bending Vibrator Consisting of a LiNbO 3 Plate with a Ferroelectric Inversion Layer. *Jpn. J. Appl. Phys.* **1987**, *26*, 198, doi:https://dx.doi.org/10.7567/JJAPS.26S2.198.

29. Standards on Piezoelectric Crystals, 1949. *Proc. IRE* **1949**, *37*, 1378–1395, doi:10.1109/JRPROC.1949.229975.

30. Weis, R. S.; Gaylord, T. K. Lithium niobate: Summary of physical properties and crystal structure. *Appl. Phys. A* **1985**, *37*, 191–203, doi:10.1007/BF00614817.

31. Sanna, S.; Schmidt, W. G. Lithium niobate X-cut, Y-cut, and Z-cut surfaces from ab initio theory. *Phys. Rev. B* **2010**, *81*, 214116.

32. Ohnishi, N. An Etching Study on a Heat-Induced Layer at the Positive-Domain Surface of LiNbO 3. *Jpn. J. Appl. Phys.* **1977**, *16*, 1069.

33. Nakamura, K.; Ando, H.; Shimizu, H. Ferroelectric domain inversion caused in LiNbO3 plates by heat treatment. *Appl. Phys. Lett.* **1987**, *50*, 1413–1414, doi:10.1063/1.97838.

34. Kugel, V. D.; Rosenman, G.; Shur, D. Piezoelectric properties of bidomain LiNbO3 crystals. *J. Appl. Phys.* **1995**, *78*, 5592–5596, doi:10.1063/1.359681.

35. Nassau, K.; Levinstein, H. J.; Loiacono, G. M. The domain structure and etching of ferroelectric lithium niobate. *Appl. Phys. Lett.* **1965**, *6*, 228–229, doi:10.1063/1.1754147.

36. Nakamura, K.; Shimizu, H. Hysteresis-free piezoelectric actuators using LiNbO3 plates with a ferroelectric inversion layer. *Ferroelectrics* **1989**, *93*, 211–216, doi:10.1080/00150198908017348.

37. Bykov, A. S.; Grigoryan, S. G.; Zhukov, R. N.; Kiselev, D. A.; Ksenich, S. V; Kubasov, I. V; Malinkovich, M. D.; Parkhomenko, Y. N. Formation of bidomain structure in lithium niobate plates by the stationary external heating method. *Russ. Microelectron.* **2014**, *43*, 536–542, doi:10.1134/S1063739714080034.

38. Blagov, A. E.; Bykov, A. S.; Kubasov, I. V; Malinkovich, M. D.; Pisarevskii, Y. V; Targonskii, A. V; Eliovich, I. A.; Kovalchuk, M. V An electromechanical x-ray optical element based on a hysteresis-free monolithic bimorph crystal. *Instruments Exp. Tech.* **2016**, *59*, 728–732, doi:10.1134/S0020441216050043.

39. Smits, J. G.; Dalke, S. I.; Cooney, T. K. The constituent equations of piezoelectric bimorphs. *Sensors Actuators A Phys.* **1991**, *28*, 41–61, doi:https://doi.org/10.1016/0924-4247(91)80007-C.

40. Kushibiki, J.; Takanaga, I.; Komatsuzaki, S.; Ujiie, T. Chemical composition dependences of the acoustical physical constants of LiNbO3 and LiTaO3 single crystals. *J. Appl. Phys.* **2002**, *91*, 6341–6349, doi:10.1063/1.1467608.

41. Zhaoqiang, C.; Huaduo, S.; Weiliang, S.; Guoxi, L.; Jingen, W.; Jikun, Y.; Shuxiang, D. Enhanced Resonance Magnetoelectric Coupling in (1.1) Connectivity Composites. *Adv. Mater.* **2017**, *29*, 1606022, doi:10.1002/adma.201606022.

42. Zhuang, X.; Sing, M. L. C.; Cordier, C.; Saez, S.; Dolabdjian, C.; Das, J.; Gao, J.; Li, J.; Viehland, D. Analysis of Noise in Magnetoelectric Thin-Layer Composites Used as Magnetic Sensors. *IEEE Sens. J.* **2011**, *11*, 2183–2188, doi:10.1109/JSEN.2011.2114648.

43. Fang, C.; Ma, J.; Yao, M.; Di, W.; Lin, D.; Xu, H.; Wang, W.; Luo, H. Equivalent magnetic noise reduction at high frequency range due to polarized direction optimization in Terfenol-D/Pb(Mg1/3Nb2/3)O3-PbTiO3 magnetoelectric laminate sensors. *J. Magn. Magn. Mater.* **2017**, *423*, 106–110, doi:https://doi.org/10.1016/j.jmmm.2016.09.074.